Check for updates

Age-related differences in cerebral blood flow and cortical thickness with an application to age prediction

M. Ethan MacDonald[a,b,c,d,∗], Rebecca J. Williams[a,b,c,d], Deepthi Rajashekar[a,b,c,d], Randall B. Stafford[a,b,c], Alexadru Hanganu[a,b,c,d], Hongfu Sun[a,b,c,d], Avery J.L. Berman[a,b,c,d,e], Cheryl R. McCreary[a,b,c,d,f], Richard Frayne[a,b,d,f], Nils D. Forkert[a,b,c,d], G. Bruce Pike[a,b,c,d]

[a] Department of Radiology, University of Calgary, Calgary, Alberta, Canada
[b] Department of Clinical Neurosciences, University of Calgary, Calgary, Alberta, Canada
[c] Healthy Brain Aging Lab, University of Calgary, Calgary, Alberta, Canada
[d] Hotchkiss Brain Institute, University of Calgary, Calgary, Alberta, Canada
[e] Department of Radiology, Athinoula A. Martinos Center for Biomedical Imaging, Harvard Medical School, Massachusetts General Hospital, Charlestown, MA, USA
[f] Seaman Family Magnetic Resonance Research Centre, Calgary, Alberta, Canada

ARTICLE INFO

ABSTRACT

Cerebral cortex thinning and cerebral blood flow (CBF) reduction are typically observed during normal healthy aging. However, imaging-based age prediction models have primarily used morphological features of the brain. Complementary physiological CBF information might result in an improvement in age estimation. In this study, T1-weighted structural magnetic resonance imaging and arterial spin labeling CBF images were acquired in 146 healthy participants across the adult life span. Sixty-eight cerebral cortex regions were segmented, and the cortical thickness and mean CBF were computed for each region. Linear regression with age was computed for each region and data type, and laterality and correlation matrices were computed. Sixteen predictive models were trained with the cortical thickness and CBF data alone as well as a combination of both data types. The age explained more variance in the cortical thickness data (average R^2 of 0.21) than in the CBF data (average R^2 of 0.09). All 16 models performed significantly better when combining both measurement types and using feature selection, and thus, we conclude that the inclusion of CBF data marginally improves age estimation.

1. Introduction

Aging is known to affect the morphology and physiology of the brain (Amin-Hanjani et al., 2014; Salat et al., 2004). In particular, cortical thickness (Lemaitre et al., 2012) and cerebral blood flow (CBF) (Rodgers et al., 2016) have been shown to decline with age. One study explored how both gray matter volume and CBF change with age (Chen et al., 2011a), and demonstrated reductions in cerebral cortex volume and CBF, and a lower rate of volume reduction in subcortical structures. The rate of thinning is also known to vary between different regions of the cortex (Lemaitre et al., 2012), while the spatial pattern of the rate of CBF reduction has not been examined in detail across cortical regions. Age prediction has been performed using brain morphology measurements in previous studies (Franke et al., 2012, 2013, 2015; Gaser et al., 2013; Valizadeh et al., 2017). In these studies, features of the brain structure, such as ventricular volume or cortical thickness, are used to estimate the chronological age of the participants using a trained predictive regression model. There are a number of applications of age prediction modeling including detection and estimation of the severity of various neurodegeneration diseases. However, segmentation of the cortex into fine structures and exploration of the regional changes with age on both cortical thickness and CBF in a cross-sectional lifespan population study have not been reported. Nor has the combination of regional cortical thickness and CBF been explored for age prediction modeling to determine if additional predicative power can be achieved.

Age is a risk factor for increased disease burden, decreased physical fitness, and reduced cognitive performance. Furthermore, physical fitness and cognition are known to negatively correlate with age, as studies have shown a robust relationship between cognition and VO_2 max during aging (Bherer et al., 2013; Kirk-

Sanchez and McGough, 2014; Wendell et al., 2014). In the study of normal aging, generally, efforts are made to select participants free of disease and cognitive deficiencies. A number of age-related diseases such as cardiovascular disease and dementia come with changes to cortical thickness and CBF (Fein et al., 2000; Fox and Schott, 2004; Román et al., 2002; Ruitenberg et al., 2005). Thus, investigating normal aging requires screening for disease and cognitive impairment to ensure a healthy aging population. Neuropsychiatric tests, self-reported medical history, and inspection of image data for incidental findings are other ways to help ensure that participants are aging healthfully (i.e., not impaired by confounding diseases). Nonetheless, it can be difficult or impossible to identify and exclude patients in the pre-symptomatic phase of certain disease of aging.

The pathophysiological relationship between cortical thinning and blood flow reduction with aging remains unclear because it is difficult to disentangle these effects empirically. Correlation between cortical thinning and CBF reduction likely exists, as both measures decline with age in a somewhat linear fashion. However, previous studies did not aim to investigate this specific relationship in detail. In the case of white matter, volumes are shown to remain constant with age (Chen et al., 2013; Good et al., 2002) while white matter CBF is difficult to reliably measure with arterial spin labeling (ASL) (Alsop et al., 2015). Thus, CBF studies are practically limited to gray matter regions.

For regional analysis of cortical thickness and CBF, an important consideration is the method used for segmenting brain structures, and there are a number of atlases available for separating the brain into different anatomical regions (Balafar et al., 2010; Desikan et al., 2006; Evans et al., 2012). Generally, a first step is to segment gray and white matter in high-resolution anatomical T1-weighted magnetic resonance imaging (MRI) datasets (Balafar et al., 2010). The cortex can be further subdivided into hemispheres and 4 lobes per hemisphere. Vascular territory mapping is also possible with advanced vessel-selective CBF measurements, whereby the brain is subdivided into watershed regions of each vascular territory (Pexman et al., 2001; Tatu et al., 1998). However, due to high inter-participants differences between vascular territories and potential mixing effects leading to overlap of territories, such a subdivision is difficult for group analysis as the watersheds can be significantly different between participants (Chappell et al., 2010; Jung, 2012; Wong, 2007). Subdividing the cortex based on anatomical regions is not only a common method for volumetric or thickness assessments, it is also acceptable for regional CBF analyses. One widely used atlas for this purpose is the Desikan-Killiany atlas, available in the FreeSurfer processing pipeline, which separates the cerebral cortex into 34 regions per hemisphere (Desikan et al., 2006), and has been shown to be a robust automated strategy. Although the cortex can be parsed into even finer regions (Destrieux et al., 2010), the low resolution and signal to noise ratio (SNR) characteristic of ASL CBF data make small regions of interest inappropriate.

To better characterize the features used when modeling, an investigation of laterality and correlation coefficients can also be conducted. Blood flow in the brain is known to have some hemispheric laterality (i.e., asymmetry), varying between different regions of the brain (Chen et al., 2011a; MacDonald and Frayne, 2015). Compared to CBF, cortical thickness shows a lesser degree of laterality (MacDonald et al., 2018b). Cortical thickness is often used to calculate a correlation matrix (Chen et al., 2011b; Gong et al., 2012), showing the relationships between thickness in the different cortical regions. To our knowledge, such a matrix has not been obtained for regional CBF measurements.

Age prediction from brain morphology has been investigated by several groups and has been suggested to be a surrogate measure of brain health by comparing estimated age with chronological age (Franke et al., 2010; Gaser et al., 2013; Tustison et al., 2014; Valizadeh et al., 2017). However, these studies are usually limited to regional volumes determined using anatomical T1-weighted MRI data. Previous works have indicated that the incorporation of functional connectivity could improve age prediction (Liem et al., 2017; Tian et al., 2016). In 2016, Cherubini et al. (2016) used a multimodal feature space including T1 anatomical, T2* relaxometry and diffusion tensor imaging, and showed that their multimodal approach was better than an individual modality. Since it is well known that blood flow also declines with age, it may provide additional information to more accurately estimate age from MRI data. There are many predictive modeling algorithms available and each is known to handle datasets with varying performance depending on the unique characteristics of data (Kuhn and Johnson, 2013).

The aim of this work is to determine if regional CBF measurements in combination with cortical thickness measurements can improve the prediction of brain age compared to using cortical thickness alone. We hypothesized that the addition of regional CBF data would improve age prediction accuracy. This study assessed the feature space of regional cortical thickness and CBF measurements across the healthy adult lifespan, to determine rates of decline with age, as well as the laterality and correlation matrices. Group analysis of CBF reduction was also performed with the aim of revealing how the blood flow changes on a voxel-wise basis. Age prediction with the incorporation of both regional cortical thickness and CBF was undertaken to understand how various predictive models would perform using one versus both measures when estimating the chronological age of healthy participants.

2. Methods

2.1. Study cohort

As part of an ongoing population study, the Calgary normative study, participants were recruited from the local Calgary community through poster advertising. This study was approved by the University of Calgary Research Ethics Board and informed written consent was obtained from all participants. Participants underwent an MRI session, completed a Montreal Cognitive Assessment (Nasreddine et al., 2005), and provided a brief medical history. Data were included if participants had an MoCA score >25 and reported no significant neurological or psychiatric history. All MRI data were also visually screened for incidental findings and quality control. After quality control, data from 146 participants (58 men, 88 women; 18—87 years) were included. The age distribution is shown in Fig. 1.

2.2. Magnetic resonance imaging

All imaging data were collected at a single center using a 3T MRI (Discovery 750; GE Healthcare) and a 12-channel neurovascular head coil. T1-weighted anatomical and ASL images were acquired for this analysis. The T1-weighted magnetization prepared rapid gradient echo mam scan had an isotropic image resolution of 1 mm and was acquired with inversion time (TI)/repetition time (TR)/echo time (TE)/flip angle (α) of 650/5.84/2.36 ms/8°. The 3-dimensional pseudo-continuous ASL was acquired with 30 slices, each 5-mm thick, and a spiral readout trajectory with an effective in-plane resolution of 2.33 mm. Label duration and post label delay were 1450 and 2025 ms, respectively (values close to those recommended by the ASL consensus white paper; Alsop et al., 2015). In addition, an M0 reference image was collected and used along with the ASL images to calculate absolute CBF (Alsop et al., 2015).
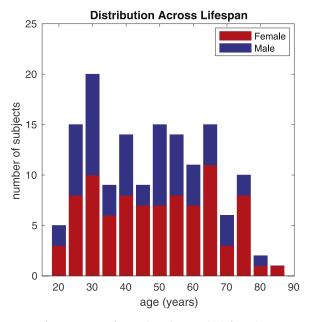
Fig. 1. Summary of age and sex demographic information.

2.3. Processing and measurements

T1-weighted images were processed using the recommended pipeline in FreeSurfer version 5.3.0 (http://surfer.nmr.mgh.harvard.edu/). The cerebral cortex was segmented and parcellated into 34 regions per hemisphere using the Desikan-Killiany (Desikan et al., 2006) atlas. Processing was performed by running the *recon-all* function, which is a standard call to process anatomical data with FreeSurfer. Briefly, the FreeSurfer pipeline for segmentation and cortical parcellation involves skull stripping (Ségonne et al., 2004), registration to a template space (Collins et al., 1994), intensity normalization (Sled et al., 1998), white matter segmentation, tessellation of the gray matter-white matter boundary, and automated topology correction (Ségonne et al., 2007; Fischl et al., 2001). The tessellated surfaces are used to define the inner and outer white matter boundaries, which are required for the calculation of cortical thickness (Dale et al., 1999; Dale and Sereno, 1993; Fischl and Dale, 2000). Following surface inflation (Fischl et al., 1999), cortical parcellation with respect to gyral and sulcal structure is performed (Desikan et al., 2006; Fischl et al., 2004). Cortical thickness is calculated as the closest distance from the gray-white boundary to the gray-cerebral spinal fluid boundary at each vertex on the tessellated white matter surface (Fischl and Dale, 2000). Average thickness was calculated for each parcellated region and for each hemisphere, resulting in 70 measurements per participants. All cortical segmentations were manually inspected for errors and 1 participant was removed from the analysis due to poor segmentation quality. The processing was performed on a parallel computer cluster (Cedar Cluster, Compute Canada; operating with CentOS and a 3.6 petaflop capacity, jobs ran on nodes with Intel E5-2683 v4 "Broadwell" 2.1 GHz processors).

Partial volume error correction was conducted by using the method described in 2017 by Zhao et al. (2017), using the tissue probability maps to solve for the CBF in the gray matter (GM) and white matter (WM) components yielding 2 maps of CBF. Tissue probability maps were calculated using the FSL's FAST algorithm (Zhang et al., 2001) on the T1-weighted images and then registered with an affine transformation to the CBF images using Advanced Normalization Tools (ANTs) (Avants et al., 2011). A 3 × 3 kernel was used to consider the WM and GM probabilities in the surrounded

voxels. A 9 × 2 equation was used along with the 9 CBF values for a system of equations to solve for the GM and WM component CBF; only the GM values were used in the next parts of the analysis.

CBF images were registered with an affine transformation to the participant-specific T1-weighted images, and the same parcellated cortical regions used for thickness estimation were used to determine the corresponding regional mean CBF. Twenty-one participants were removed due to insufficient CBF image quality (motion, poor registration, or other artifacts); this combined with the participant removed for poor image quality left the study with 146 participants in the analysis.

To visualize the CBF reduction with age over the whole brain on a voxel-wise basis, the ASL images (prior to CBF calculation) were also registered to the International Consortium for Brain Mapping atlas (Mazziotta et al., 2001) employing a non-linear registration, so that group averages and voxel-wise regression maps could be computed. All registrations were implemented with ANTs v2.2 using a mutual information cost function and linear interpolation, and manually inspected for errors and, where appropriate, constraints were adjusted to improve registration accuracy.

2.4. Analysis of feature space

Linear regression was performed for each cortical region and for each data type and the R^2 was recorded to investigate how much of the variation in thickness and CBF could be explained by age. Spearman correlation tests were calculated to investigate the relationship between cortical thickness and CBF versus age for each region and to determine if there was a significant effect of age. Spearman was used instead of Pearson correlation because it does not assume any underlying distribution. Regions meeting $p < 0.05$ and $p < 0.0007$ significance levels were recorded. Laterality index was computed between the left and right hemispheres as (L−R)/(L+R) for regions of each data type. A multivariate analysis of covariance (MANCOVA) test was then run to determine the effect of sex with a $p < 0.01$ considered significant.

A hierarchical analysis was performed by calculating the R^2 for several subdivisions of the CBF gray matter, including all of gray matter, 2 hemispheres, 8 hemispheric lobes, and 68 cortical regions. The average regression coefficient (R^2) was then computed at each hierarchical level. This analysis sheds light on the effect of separating the CBF features into smaller and smaller regions.

Finally, correlation matrices of cortical thickness and CBF measurements were computed for all regions. The Shannon entropy of the Eigen spectrum of these correlation matrices was calculated, $(H(A) = -\sum_i \lambda_i \log_2 \lambda_i$, where λ_i is the ith Eigen component of matrix A), where uncorrelated predictors would have an entropy of 0 and a full correlation of 68 predictors would have an entropy of −413.9. A correlation between cortical thickness and CBF measurements was performed to determine how much variance was shared between the 2 data types.

2.5. Predictive models

Several predictive models were trained to estimate the chronological age of participants given 3 cases of the data: (1) cortical thickness only, (2) CBF only, and (3) both. Models were built and trained using R (version 3.5.0) (R Core Team, 2018) and processing was performed on the same compute cluster mentioned above. The 16 most common regression model types used for age prediction were tested: (1) multiple linear regression (MLR) (Graybill, 1976), (2) partial least squares (PLS) (Stone and Brooks, 1990; Wold, 1966; Wold et al., 1987), (3) ridge regression (RR) (Hoerl and Kennard, 1970), (4) elastic net (ENET) (Hui and Trevor, 2005), (5) neural network (NN) (Bishop and Bishop, 1995; Michael, 2010; Ripley,

2007), (6) multivariate adaptive regression splines (Friedman, 1991), (7–9) linear, radial basis function, and polynomial support vector machine (lSVM, rSVM, pSVM) (Drucker et al., 1997; Smola, 1996), (10) k-nearest neighbors (Altman, 1992), (11) simple classification and regression tree (Breiman et al., 1984; Leo et al., 1984), (12) decision tree with regression at the nodes (M5) tree (Wang and Witten, 1996), (13) bagged trees (Breiman, 1996), (14) random forest (Breiman, 2001), (15) boosted trees (Friedman, 2001), and (16) cubist (Quinlan, 1987, 1992, 1993). Many model types were selected to assess the generalizability of feature space to predict age (Kuhn and Johnson, 2013). Many of the models had one or more parameters that required tuning, which was performed across a tuning grid. Features were scaled to appropriate dynamic ranges for each model type, and hyperparameters were tuned in inner cross validations. The parameters were optimized by minimizing the root mean square error employing a leave-one-out cross validation. To evaluate the performance of each model, the coefficient of determination (R^2) corresponding to the optimal root mean square error was recorded. Due to the smaller group size, no hold out dataset was used.
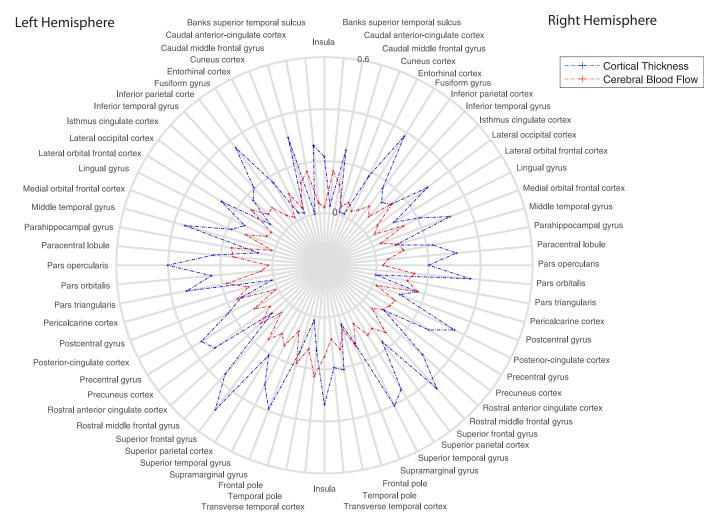
For feature selection, the features were ranked with ReliefF (Robnik-Šikonja and Kononenko, 2003), and sequentially removed. With this methodology, the features are ranked with the ReliefF algorithm and the lowest ranked feature is removed and then the process stated in the above paragraph is repeated. This process is repeated until there is only one feature left. The feature set that yields the lowest root mean square error is then considered to be the optimal feature set for the given method. R^2 results with and without feature selection are reported to determine the effect of feature selection with respect to improvements in model performance.

The outcomes from the predictive models were used to test the hypothesis that combining CBF data with cortical thickness data would provide a better estimate of age than using the cortical thickness or CBF data alone. The residuals of the cortical thickness and CBF measurements, as well as residuals from the models using cortical thickness and models made of both measurement types were compared with a Friedman test and a $p < 0.0007$ was considered significant. The Friedman test was selected as it is used to detect differences between multiple test attempts. Tests were also performed between the cortical thickness and CBF models to test if one data type performed significantly better.

3. Results

Fig. 2 shows a polar plot to illustrate the differences in regional R^2 with age for the cortical thickness and CBF data. In general, the R^2

Fig. 2. Polar plot indicating the R^2 regression with age parameter of the cortical thickness (blue) and cerebral blood flow (red) in 68 cortex regions. For the vast majority of the regions, the cortical thickness measurements have higher R^2 than the cerebral blood flow measurements. (For interpretation of the references to color in this figure legend, the reader is referred to the Web version of this article.)

is lower for the CBF data, which indicates that less of the variance in the CBF data can be explained by age. The average R^2 for the cortical thickness regressions is 0.21, while the average R^2 for the CBF regressions is 0.09. When considering all regions, 49 regions have a higher R^2 in the cortical thickness measurements, while only 19 regions have a higher R^2 in the CBF measurements. In cases where the R^2 is higher for the CBF regressions, these measurements tended to occur in regions where cortical thickness is known to be affected less by age (Lemaitre et al., 2012), and the CBF tends to reduce at a more equal level independent of the region. The Spearman correlation tests of cortical thickness versus age yield 59/68 statistically significant regions at $p < 0.05$ and 55/68 regions at $p < 0.0007$, while 61/68 CBF measurements had a statistically significant regression with age at $p < 0.05$ and 40/68 at $p < 0.0007$. These tests indicate that even with a very high multiple comparisons correction factor, many of these regressions are still significant. MANCOVA tests indicated statistically significant differences between male and females ($p < 0.01$).
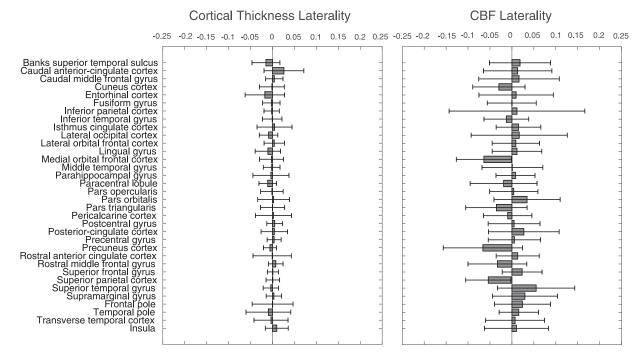
For the hierarchical analysis, the average R^2 was 0.112, 0.109, 0.101, and 0.093; for all of gray matter, the 2 hemispheres, 8 hemispheric lobes, and 68 cortical regions, respectively. There is a small reduction in the R^2 when comparing all of gray matter to the 68 cortical regions; however, in the latter case there are many more measured features available for modeling. This result suggests that finer selection of the regions will yield more useful features with only a slightly lower R^2.

Figs. 3 and 4 show the laterality indices and correlation matrices, respectively. CBF measurements had more laterality and were more highly correlated across regions than cortical thickness measurements. Structural correlation matrices have been shown in previous studies (Chen et al., 2011a; Gong et al., 2012), and this matrix is consistent with those reported previously. The Shannon entropy of the Eigen spectrum from the correlation matrices yielded −143.9 and −274.3 for the cortical thickness and CBF data types, respectively, reflecting greater correlation between regions in the CBF data.
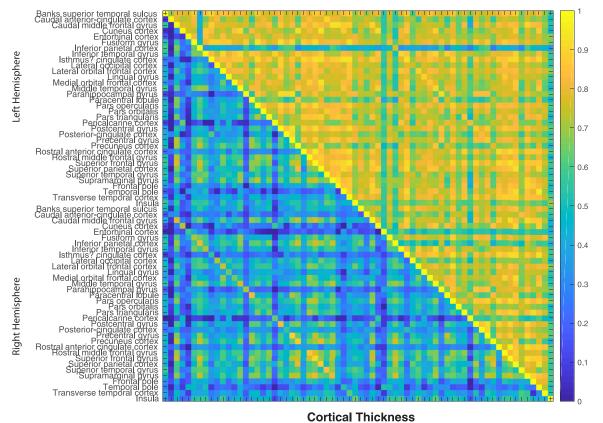
Fig. 5 shows result of registering all CBF images to atlas space and computing the regression on a voxel-wise basis, yielding CBF group average and regression maps. Generally, the rate of change is higher in cortical gray matter, and slightly lower in subcortical gray matter. There is effectively no change in white matter; however, the method used to measure CBF does not provide reliable white matter perfusion estimates. The consistent rate of CBF reduction with age across the cortical gray matter is consistent with correlations observed in Fig. 4, as perfusion in all cortical regions is reducing from a similar level at the similar rate. Although we report an intercept map from the linear regression, CBF is known to have a non-linear property during the developmental years between birth and late teenage years (Ogawa et al., 1989). Thus, these numbers should not be used to extrapolate over that range. R^2 was largest near the feeding vessels (middle cerebral artery, anterior cerebral artery). In the supplemental data please find the computed regression maps.

Fig. 6 shows the performance of the 16 predictive models. pSVM performed best with an R^2 of 0.63 and 0.64, without and with feature selection, respectively. The feature rankings are shown in Table 1. The pSVM model had a mean absolute error of 7.8 and 7.5 years, without and with feature selection, respectively. The first 8 methods all performed slightly better when including CBF measurements, as opposed to using just cortical thickness measurements (pSVM, RR, ENET, PLS, boosted trees, cubist, rSVM, and bagged trees). In general, most of the models had similar performance when including just the cortical thickness data. Without feature selection, R^2 ranged between 0.43 and 0.61, while models trained with CBF data only had more variation in their performance with R^2 ranging between 0.16 and 0.54. Feature selection resulted in small improvements in many of the methods but had a large impact on the MLR model. The age estimates for the best performing model is shown in Fig. 7.

A summary of the Friedman tests is shown in Table 2. There were no statistical differences found between the cortical thickness and CBF residuals, despite the large deviations in the R^2. Without

Fig. 3. Hemispheric laterality indices for cortical thickness and CBF. Laterality index = (L−R)/(L + R). Plotted are mean (gray bar) and standard deviation (error bars). Abbreviation: CBF, cerebral blood flow.

Cerebral Blood Flow

Fig. 4. Correlation matrix of cortical thickness (lower left diagonal) and cerebral blood flow (upper right diagonal). Since the correlation matrices are symmetrical only half of each matrix is shown and the 2 are concatenated. The cerebral blood flow data are more highly correlated than the cortical thickness.

feature selection, the cubist, NN, and simple classification and regression tree models had significantly better performance when using the combined feature set compared to the cortical thickness features alone. With feature selection, 5 models did perform significantly better—the pSVM, ENET, PLS, boosted trees, and multivariate adaptive regression spline models.
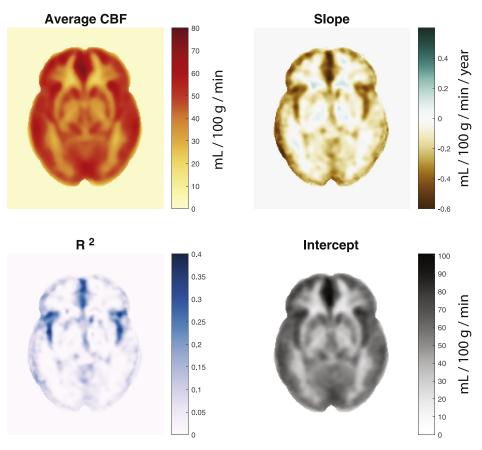
4. Discussion

Our results demonstrate that CBF can be used to improve age estimation compared to cortical thickness alone. Although the differences are small, there are significant improvements for many of the models considered here, according to the Friedman tests, demonstrating that CBF does add additional information that can improve age prediction. Including CBF data in more sophisticated age prediction models, such as deep learning (Cole et al., 2017), convolutional NN (Li et al., 2018), and generalized Gaussian processes (Gutierrez Becker et al., 2018), may show further improvements. Additionally, the inclusion of CBF in age prediction should increase sensitivity to diseases with reduced blood flow, such as aneurysm (MacDonald et al., 2015, 2016) and as Alzheimer's disease (Roher et al., 2012). The utility of the current work also lies in the characterization of the feature space, with regression, correlation, and laterality. Normative CBF and cortical thickness rate changes were presented (a regression map of the CBF rate of change is provided in the supplemental materials). This work also demonstrates a framework for assessing the performance of an additional modality to age prediction.
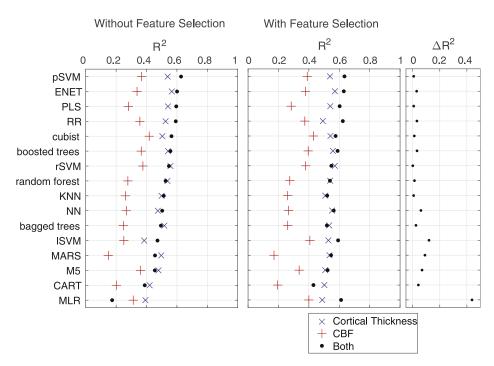
The results of this study lead to a few generalizable observations, including: (1) aging was associated with lower R^2 in CBF data than cortical thickness, (2) there is more laterality in cortical CBF than cortical thickness, (3) CBF is more correlated between regions than cortical thickness, (4) group average maps indicate that the reduction of CBF with age is constrained primarily to gray matter with similar rates of change across regions, (5) age prediction can perform slightly better with the inclusion of CBF data when a suitable model type is used, and (6) feature selection improves age prediction modeling. Of course, results may vary slightly with different population samples or acquisition parameters not explored in this study.

We found that more variance can be explained by age in the cortical thickness than CBF. This finding can be rationalized as CBF measurements have more physiological variance unrelated to aging than cortical thickness measurements, such as variable cardiac output, caffeine consumption, fitness levels, and blood CO_2 levels (Berman et al., 2018). Methodological issues such as lower SNR and resolution of the ASL image data are also factors that may contribute to this result.

Compared to previous similar studies of cortical thickness and CBF (Lemaitre et al., 2012; MacDonald and Frayne, 2015), this study adds new information including the predictive analysis. It has been reported that cortical thickness changes are typically bilateral, and often, only the bilateral average cortical thickness values are reported (Lemaitre et al., 2012). CBF measurements exhibit more laterality than cortical thickness (Chen et al., 2011a; MacDonald and Frayne, 2015). There was a high degree of correlation in the CBF measurements, an average coefficient of 0.73 (as opposed to 0.40 in

Fig. 5. Group analysis of CBF versus age map. In addition to calculating the average CBF, a regression was performed on each voxel to obtain the slope, R^2, and intercept. The gray matter cortical regions have a decrease of 0.4–0.6 mL/100 g/min/y. Abbreviation: CBF, cerebral blood flow.

Fig. 6. Performance of predictive models. Three sets of data were used to calibrate each model, the blue × uses the cortical thickness data, the red plus sign uses the CBF data, and the black dot uses both the cortical thickness and CBF data. The model types are sorted from by the performance with the combined dataset. The right most plot shows the change in the R^2 with feature selection. Abbreviations: CART, simple classification and regression tree; ENET, elastic net; KNN, k-nearest neighbors; lSVM, linear support vector machine; MARS, multivariate adaptive regression splines; MLR, multiple linear regression; NN, neural network; PLS, partial least squares; pSVM, polynomial support vector machine; RR, ridge regression; rSVM, radial support vector machine. (For interpretation of the references to color in this figure legend, the reader is referred to the Web version of this article.)

Table 1
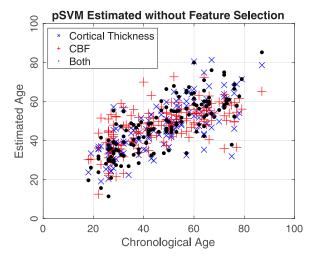Top 15 ranked features using the feature selection for each data type

Rank	Top cortical thickness features	Top CBF features
1	lh-Insula	lh-Transverse temporal cortex
2	lh-Frontal pole	lh-Caudal middle frontal gyrus
3	lh-Lingual gyrus	rh-Caudal middle frontal gyrus
4	rh-Insula	lh-Caudal anterior cingulate cortex
5	rh-Medial orbital frontal cortex	lh-Superior parietal cortex
6	lh-Superior parietal cortex	lh-Average
7	lh-Rostral anterior cingulate cortex	rh-Fusiform gyrus
8	rh-Middle temporal gyrus	lh-Rostral anterior cingulate cortex
9	rh-Pars triangularis	lh-Fusiform gyrus
10	rh-Superior frontal gyrus	rh-Cuneus cortex
11	lh-Precentral gyrus	lh-Posterior cingulate cortex
12	rh-Superior parietal cortex	lh-Rostral middle frontal gyrus
13	rh-Lateral orbital frontal cortex	rh-Middle temporal gyrus
14	rh-Rostral anterior cingulate cortex	lh-Banks superior temporal sulcus
15	lh-Rostral middle frontal gyrus	lh-Inferior temporal gyrus

Key: lh, left hemisphere; rh, right hemisphere.

cortical thickness), which implies that if blood flow in any one region is reduced, a similar effect is seen in all other regions. The Shannon entropy of the Eigen spectrum from the correlation matrices yielded −143.9 and −274.3 for the cortical thickness and CBF data types, respectively (fully uncorrelated predictors would have an entropy of 0, while a full correlation of 68 predictors would have an entropy of −413.9). From this result, it is clearly more beneficial to parcellate the cortical thickness as opposed to the CBF data, as each regional cortical thickness measurement has more independent information than a regional CBF measurement.

Due to the scope of the experiment, there are many limitations, such as the methods used to acquire the data, particularly ASL which has many nuanced methodologies, as well as the choice of population and choices regarding the processing pipeline. CBF is heavily sensitized to the blood arrival time, and future work might reveal this is a significant source of the change in CBF.

Cortical thickness and CBF measurements are not necessarily changing linearly with age, particularly in the younger age ranges (Ogawa et al., 1989). Due to the variability in the data and relatively small sample size, a linear approximation is appropriate. Inclusion of more participants would allow a more precise piecewise linear or non-linear modeling method. Linear regression is also susceptible to leveraging (particularly when there is a non-uniform age

distribution), whereby a point at the beginning or end of the sample skews the regression. Although there are some quantitative methods for commuting regression leverage of each of the points, visual inspection of the plots will often suffice and so we inspected each of the regression plots for leveraging effects but did not need to remove any outliners.

Sex-based differences also exist for both cortical thickness and CBF. In our datasets, MANCOVA tests indicated statistically significant differences between male and females ($p < 0.001$). So, incorporation of sex as a feature into some models would intuitively improve prediction. Incorporating sex into some models such as MLR is more nuanced, as it is a binary input and the model only takes continuous variables. A strategy around this would be to train different models for each sex; however, this would require more participants as there would be twice the number of parameters in the model. Furthermore, there are many other parameters, which could also be incorporated into our models such as handedness, smoking status, physical fitness, ethnicity, genetic markers, and so on. However, a larger sample size and uniform sampling across these features would be required to explore these features systematically. In this work, we aimed to produce a model that uses only brain mapping features and have excluded these other effects.

Machine learning models use training data, and this data can be seen as the experience of the model. Thus, all methods are limited by the quality of the training data. In this experiment, we have made an effort to have a representative healthy population, by ensuring there are no major neurological or cognitive impairments. There is potential for many conditions which may skew an individual in the population to have either a particularly low or high features, such as Alzheimer's disease or a particularly robust cerebrovascular system into late life, respectively. In fact, some brain age prediction models use the deviation in the chronological age and estimated age as an indicator of neurodegeneration (Gaser et al., 2013). A model using only the CBF features would thus be more sensitive to changes in the cerebrovascular health, and the combined models would be sensitive to both brain structure and cerebrovascular health.

The number of participants included in this study is not as large as some other recent studies that aim to develop and evaluate predictive models of age, based only on morphological features; databases with between approximately 1000−3000 participants have yielded an R^2 of closer to 0.8 or 0.9, and mean absolute differences between 4 and 5 (MacDonald et al., 2018b; Valizadeh et al., 2017). The aim of this paper is not to achieve lower mean absolute errors than previous studies. Rather, we sought to investigate the

Fig. 7. Estimated age versus chronological age for the best trained model. Abbreviations: CBF, cerebral blood flow; pSVM, polynomial support vector machine.

Table 2
Friedman test outcomes

Machine learning type	No feature selection		Feature selection	
	CBF - cortical thickness	Cortical thickness - both	CBF - cortical thickness	Cortical thickness - both
pSVM	*p* < 0.0007	*p* < 0.0007	*p* < 0.0007	*p* < 0.0007
ENET	*p* < 0.0007	*p* < 0.0007	*p* < 0.0007	*p* < 0.0007
RR	*p* < 0.0007	*p* < 0.0007	*p* < 0.0007	*p* < 0.0007
PLS	*p* = 0.0282	*p* < 0.0007	*p* < 0.0007	*p* < 0.0007
rSVM	*p* = 0.0007	*p* < 0.0007	*p* < 0.0007	*p* < 0.0007
Cubist	*p* = 0.0008	*p* < 0.0007	*p* < 0.0007	*p* < 0.0007
Boosted trees	*p* < 0.0007	*p* < 0.0007	*p* < 0.0007	*p* < 0.0007
NN	*p* < 0.0007	*p* < 0.0007	*p* < 0.0007	*p* < 0.0007
Random forest	*p* < 0.0007	*p* < 0.0007	*p* < 0.0007	*p* < 0.0007
M5	*p* < 0.0007	*p* < 0.0007	*p* < 0.0007	*p* < 0.0007
Bagged trees	*p* < 0.0007	*p* < 0.0007	*p* < 0.0007	*p* < 0.0007
KNN	*p* = 0.0562	*p* = 0.0056	*p* < 0.0007	*p* < 0.0007
MARS	*p* < 0.0007	*p* < 0.0007	*p* < 0.0007	*p* < 0.0007
lSVM	*p* = 0.0021	*p* < 0.0007	*p* < 0.0007	*p* < 0.0007
CART	*p* < 0.0007	*p* < 0.0007	*p* < 0.0007	*p* < 0.0007
MLR	*p* = 0.0144	*p* = 0.3893	*p* = 0.0244	*p* < 0.0007
	CBF - cortical thickness	Cortical thickness - both	CBF - cortical thickness	Cortical thickness - both
pSVM	*p* < 0.0007	*p* < 0.0007	*p* < 0.0007	*p* < 0.0007
ENET	*p* < 0.0007	*p* < 0.0007	*p* < 0.0007	*p* < 0.0007
RR	*p* < 0.0007	*p* < 0.0007	*p* < 0.0007	*p* < 0.0007
PLS	*p* = 0.0282	*p* < 0.0007	*p* < 0.0007	*p* < 0.0007
rSVM	*p* = 0.0007	*p* < 0.0007	*p* < 0.0007	*p* < 0.0007
Cubist	*p* = 0.0008	*p* < 0.0007	*p* < 0.0007	*p* < 0.0007
Boosted trees	*p* < 0.0007	*p* < 0.0007	*p* < 0.0007	*p* < 0.0007
NN	*p* < 0.0007	*p* < 0.0007	*p* < 0.0007	*p* < 0.0007
Random forest	*p* < 0.0007	*p* < 0.0007	*p* < 0.0007	*p* < 0.0007
M5	*p* < 0.0007	*p* < 0.0007	*p* < 0.0007	*p* < 0.0007
Bagged trees	*p* < 0.0007	*p* < 0.0007	*p* < 0.0007	*p* < 0.0007
KNN	*p* = 0.0562	*p* = 0.0056	*p* < 0.0007	*p* < 0.0007
MARS	*p* < 0.0007	*p* < 0.0007	*p* < 0.0007	*p* < 0.0007
lSVM	*p* = 0.0021	*p* < 0.0007	*p* < 0.0007	*p* < 0.0007
CART	*p* < 0.0007	*p* < 0.0007	*p* < 0.0007	*p* < 0.0007
MLR	*p* = 0.0144	*p* = 0.3893	*p* = 0.0244	*p* < 0.0007

These tests show the results of the Friedman tests between residuals for different prediction models and different subsets of features. Cells that are gray indicate significance ($p < 0.0007$). With feature selection, and when including both CBF and cortical thickness data (rightmost column) all model types performed statistically better.

Key: CART, simple classification and regression tree; CBF, cerebral blood flow; ENET, elastic net; KNN, k-nearest neighbors; lSVM, linear support vector machine; MARS, multivariate adaptive regression splines; MLR, multiple linear regression; NN, neural network; PLS, partial least squares; pSVM, polynomial support vector machine; RR, ridge regression; rSVM, radial support vector machine.

additive value of CBF data using a smaller database with very consistent data (one scanner, a consistent imaging protocol, detailed quality assurance). However, having a larger database with more than 1000 participants with CBF and structural MRI data would allow for a large holdout data sample and more training data, which could yield higher R^2 than those shown in Fig. 6. Such a large single dataset is not currently available and combining multiple databases can reduce data consistency (MacDonald et al., 2018b). Due to the limited number of participants in our study we could not use a holdout dataset and therefore preformed a cross validation analysis and were conservative not to allow overfitting. A recent study considered more advanced features using a patch-based method, which outperformed all other previous studies (Beheshti et al., 2019); how effective such an approach would be with combined cortical thickness and CBF remains to be determined.

The voxel-wise regression maps (Fig. 5) are consistent with a previous study, by Chen et al. (2011a), which examined the rates of change in averaged cortical gray matter and averaged subcortical gray matter. In this study, it was found that the rate of change of CBF was higher in the cortex, and lower in the subcortical regions.

Of the different machine learning types, models which inherently penalized non-informative coefficients tended to perform better without feature selection. For example, the pSVM, RR, ENET, and PLS all penalize or reduce the effect of non-informative features and were top performing methods without feature selection, while MLR, which equally weights the features, performed poorly. So,

there was not a large improvement with feature selection in models that inherently penalized features, while there was a large improvement in some other models, particularly MLR. We previously published results using MLR with a feature reduction strategy to improve performance with cortical thickness and CBF data showing how this improvement takes place as a function of the number of features (MacDonald et al., 2018a). In this work, the ReliefF feature ranking approach was used, which is a widely used and accepted method; however, there are several other feature selection algorithms that could have been used.

This work presents a framework that can be easily expanded to further improve the age estimation by including other modalities that are known to vary with age, such as quantitative T1 and T2 mapping (Kumar et al., 2012; Steen et al., 1995), quantitative susceptibility mapping (Bilgic et al., 2012; Sun et al., 2018), diffusion imaging (Chen et al., 2013; Hsu et al., 2008), and resting state functional MRI fluctuations (Ferreira and Busatto, 2013; Koch et al., 2010). However, as the number of features is increased, the required number of samples to adequately train the models also increases. Also, knowledge of the feature space will help to reduce redundant information. For example, it is known that the quantitative T1 and T2, and quantitative susceptibility mapping change with age are predominately driven by tissue iron concentration in the subcortical structures (Ogg and Steen, 1998). Thus, including more than one of these imaging modalities may provide little benefit. Similarly, phase contrast volume flow rates in the cerebral vessels are

associated with age (Amin-Hanjani et al., 2014). However, the incorporation of phase contrast flow measurements and CBF in the same predicative model may add redundant information of minimal value. Although it is best to have features be completed uncorrelated, since cortical thickness and CBF tend to be trending in a given direction with age, there is expected to be some correlation.

More variance can be explained by age in cortical thickness measurements than CBF measurements. This may be due to CBF measurements from the inherently low resolution and SNR in ASL. Furthermore, the CBF can change due to systemic physiological parameters such as heart rate, blood pressure, caffeine consumption, and blood carbon dioxide levels. Unfortunately, each of these parameters creates an additional source of variance, which may obscure the total variance that can be explained by age. However, the unexplained variance of both data types can likely be attributed to inter-participant variability from a variety of sources, and there are more of these sources contributing to CBF than cortical thickness. Furthermore, CBF is known to increase in variance with age (Amin-Hanjani et al., 2014), leading to less accurate estimates at this end of the age range.

There is more laterality in CBF than cortical thickness, yet high correlation between regional CBF values. The flow reduction maps (Fig. 5) corroborate this effect by demonstrating a consistent reduction in flow across the cortex. We have previously demonstrated blood flow laterality with phase contrast imaging (MacDonald and Frayne, 2015), and some other studies have found flow laterality in CBF measurements (Chen et al., 2011a). Similar regional flow asymmetry was found in this study. Some correlative effect is expected as both measures are reducing with age.

5. Conclusion

We measured cortical thickness and CBF changes during healthy aging and inspected their regression, correlation, and laterality to better understand the feature space. We showed that 8 of the 16 models performed slightly better at estimating chronological age when CBF was combined with cortical thickness. Depending on the performance metric considered, either max R^2 or the statistical significance, the pSVM or cubist models perform best, respectively. Careful feature interrogation, model selection, calibration, and training should be undertaken when incorporating new image feature types from alternative modalities. Although we obtained only a marginal improvement in brain age prediction with the incorporation of CBF, additional information is contained in the CBF and more advanced predictive models may further improve performance. Detection of pathologies that have an associated blood flow changes should also be enhanced with the inclusion of CBF.

Disclosure statement

The authors have no actual or potential conflicts of interest.

CRediT authorship contribution statement

M. Ethan MacDonald: Conceptualization, Methodology, Software, Validation, Formal analysis, Investigation, Resources, Data curation, Writing - original draft, Writing - review & editing, Visualization, Supervision, Project administration, Funding acquisition. **Rebecca J. Williams:** Conceptualization, Methodology, Formal analysis, Writing - review & editing, Visualization. **Deepthi Rajashekar:** Conceptualization, Methodology, Software, Writing - review & editing, Visualization. **Randall B. Stafford:** Conceptualization, Methodology, Writing - review & editing, Visualization. **Alexadru Hanganu:** Conceptualization, Methodology, Writing - review & editing, Visualization. **Hongfu Sun:** Conceptualization,

Methodology, Writing - review & editing, Visualization. **Avery J.L. Berman:** Conceptualization, Methodology, Writing - review & editing, Visualization. **Cheryl R. McCreary:** Conceptualization, Methodology, Data curation, Writing - review & editing, Visualization. **Richard Frayne:** Conceptualization, Methodology, Data curation, Writing - review & editing, Visualization, Supervision, Project administration, Funding acquisition. **Nils D. Forkert:** Conceptualization, Methodology, Resources, Data curation, Formal analysis, Investigation, Writing - original draft, Writing - review & editing, Visualization. **G. Bruce Pike:** Conceptualization, Methodology, Formal analysis, Investigation, Resources, Writing - original draft, Writing - review & editing, Visualization, Supervision, Project administration, Funding acquisition.

References

Alsop, D.C., Detre, J.A., Golay, X., Günther, M., Hendrikse, J., Hernandez-Garcia, L., Lu, H., MacIntosh, B.J., Parkes, L.M., Smits, M., van Osch, M.J.P., Wang, D.J.J., Wong, E.C., Zaharchuk, G., 2015. Recommended implementation of arterial spin-labeled perfusion MRI for clinical applications: a consensus of the ISMRM perfusion study group and the European consortium for ASL in dementia. Magn. Reson. Med. 73, 102—116.

Altman, N.S., 1992. An introduction to kernel and nearest-neighbor nonparametric regression. Am. Stat. 46, 175—185.

Amin-Hanjani, S., Du, X., Pandey, D.K., Thulborn, K.R., Charbel, F.T., 2014. Effect of age and vascular anatomy on blood flow in major cerebral vessels. J. Cereb. Blood Flow Metab. 35, 312—318.

Avants, B.B., Tustison, N.J., Song, G., Cook, P.A., Klein, A., Gee, J.C., 2011. A reproducible evaluation of ANTs similarity metric performance in brain image registration. Neuroimage 54, 2033—2044.

Balafar, M.A., Ramli, A.R., Saripan, M.I., Mashohor, S., 2010. Review of brain MRI image segmentation methods. Artif. Intelligence Rev. 33, 261—274.

Beheshti, I., Gravel, P., Potvin, O., Dieumegarde, L., Duchesne, S., 2019. A novel patch-based procedure for estimating brain age across adulthood. Neuroimage 197, 618—624.

Berman, A.J.L., Mazerolle, E.L., MacDonald, M.E., Blockley, N.P., Luh, W.-M., Pike, G.B., 2018. Gas-free calibrated fMRI with a correction for vessel-size sensitivity. Neuroimage 169, 176—188.

Bherer, L., Erickson, K.I., Liu-Ambrose, T., 2013. A review of the effects of physical activity and exercise on cognitive and brain functions in older adults. J. Aging Res. 2013, 8.

Bilgic, B., Pfefferbaum, A., Rohlfing, T., Sullivan, E.V., Adalsteinsson, E., 2012. MRI estimates of brain iron concentration in normal aging using quantitative susceptibility mapping. Neuroimage 59, 2625—2635.

Bishop, C., Bishop, C.M., 1995. Neural Networks for Pattern Recognition. Oxford University Press, Oxford, United Kingdom.

Breiman, L., 1996. Bagging predictors. Machine Learn. 24, 123—140.

Breiman, L., 2001. Random forests. Machine Learn. 45, 5—32.

Breiman, L., Friedman, J., Olshen, R., Stone, C., 1984. Classification and Regression Trees. Monterey, CA. Wadsworth. Wadsworth Statistics/Probability Series. Wadsworth Advanced Books and Software, Belmont, CA.

Chappell, M.A., Okell, T.W., Jezzard, P., Woolrich, M.W., 2010. A general framework for the analysis of vessel encoded arterial spin labeling for vascular territory mapping. Magn. Reson. Med. 64, 1529—1539.

Chen, J.J., Rosas, H.D., Salat, D.H., 2011a. Age-associated reductions in cerebral blood flow are independent from regional atrophy. Neuroimage 55, 468—478.

Chen, X., Errangi, B., Li, L., Glasser, M.F., Westlye, L.T., Fjell, A.M., Walhovd, K.B., Hu, X., Herndon, J.G., Preuss, T.M., Rilling, J.K., 2013. Brain aging in humans, chimpanzees (*Pan troglodytes*), and rhesus macaques (*Macaca mulatta*): magnetic resonance imaging studies of macro- and microstructural changes. Neurobiol. Aging 34, 2248—2260.

Chen, Z.J., He, Y., Rosa-Neto, P., Gong, G., Evans, A.C., 2011b. Age-related alterations in the modular organization of structural cortical network by using cortical thickness from MRI. Neuroimage 56, 235—245.

Cherubini, A., Caligiuri, M.E., Peran, P., Sabatini, U., Cosentino, C., Amato, F., 2016. Importance of multimodal MRI in characterizing brain tissue and its potential application for individual age prediction. IEEE J. Biomed. Health Inform. 20, 1232–1239.

Cole, J.H., Poudel, R.P.K., Tsagkrasoulis, D., Caan, M.W.A., Steves, C., Spector, T.D., Montana, G., 2017. Predicting brain age with deep learning from raw imaging data results in a reliable and heritable biomarker. Neuroimage 163, 115–124.

Collins, D.L., Neelin, P., Peters, T.M., Evans, A.C., 1994. Automatic 3D intersubject registration of MR volumetric data in standardized Talairach space. J. Comput. Assist. Tomogr. 18, 192–205.

Dale, A.M., Fischl, B., Sereno, M.I., 1999. Cortical surface-based analysis: I. Segmentation and surface reconstruction. Neuroimage 9, 179–194.

Dale, A.M., Sereno, M.I., 1993. Improved localizadon of cortical activity by combining EEG and MEG with MRI cortical surface reconstruction: a linear approach. J. Cogn. Neurosci. 5, 162–176.

Desikan, R.S., Ségonne, F., Fischl, B., Quinn, B.T., Dickerson, B.C., Blacker, D., Buckner, R.L., Dale, A.M., Maguire, R.P., Hyman, B.T., Albert, M.S., Killiany, R.J., 2006. An automated labeling system for subdividing the human cerebral cortex on MRI scans into gyral based regions of interest. Neuroimage 31, 968–980.

Destrieux, C., Fischl, B., Dale, A., Halgren, E., 2010. Automatic parcellation of human cortical gyri and sulci using standard anatomical nomenclature. Neuroimage 53, 1–15.

Drucker, H., Burges, C.J., Kaufman, L., Smola, A.J., Vapnik, V., 1997. Support vector regression machines. In: Advances in Neural Information Processing Systems, pp. 155–161.

Evans, A.C., Janke, A.L., Collins, D.L., Baillet, S., 2012. Brain templates and atlases. Neuroimage 62, 911–922.

Fein, G., Di Sclafani, V., Tanabe, J., Cardenas, V., Weiner, M.W., Jagust, W.J., Reed, B.R., Norman, D., Schuff, N., Kusdra, L., Greenfield, T., Chui, H., 2000. Hippocampal and cortical atrophy predict dementia in subcortical ischemic vascular disease. Neurology 55, 1626–1635.

Ferreira, L.K., Busatto, G.F., 2013. Resting-state functional connectivity in normal brain aging. Neurosci. Biobehav. Rev. 37, 384–400.

Fischl, B., Dale, A.M., 2000. Measuring the thickness of the human cerebral cortex from magnetic resonance images. Proc. Natl. Acad. Sci. 97, 11050–11055.

Fischl, B., Liu, A., Dale, A.M., 2001. Automated manifold surgery: constructing geometrically accurate and topologically correct models of the human cerebral cortex. IEEE Trans. Med. Imaging 20, 70–80.

Fischl, B., Sereno, M.I., Dale, A.M., 1999. Cortical surface-based analysis: II: inflation, flattening, and a surface-based coordinate system. Neuroimage 9, 195–207.

Fischl, B., van der Kouwe, A., Destrieux, C., Halgren, E., Ségonne, F., Salat, D.H., Busa, E., Seidman, L.J., Goldstein, J., Kennedy, D., Caviness, V., Makris, N., Rosen, B., Dale, A.M., 2004. Automatically parcellating the human cerebral cortex. Cereb. Cortex 14, 11–22.

Fox, N.C., Schott, J.M., 2004. Imaging cerebral atrophy: normal ageing to Alzheimer's disease. Lancet 363, 392–394.

Franke, K., Gaser, C., Manor, B., Novak, V., 2013. Advanced BrainAGE in older adults with type 2 diabetes mellitus. Front. Aging Neurosci. 5, 90.

Franke, K., Hagemann, G., Schleussner, E., Gaser, C., 2015. Changes of individual BrainAGE during the course of the menstrual cycle. Neuroimage 115, 1–6.

Franke, K., Luders, E., May, A., Wilke, M., Gaser, C., 2012. Brain maturation: predicting individual BrainAGE in children and adolescents using structural MRI. Neuroimage 63, 1305–1312.

Franke, K., Ziegler, G., Klöppel, S., Gaser, C., 2010. Estimating the age of healthy subjects from T1-weighted MRI scans using kernel methods: exploring the influence of various parameters. Neuroimage 50, 883–892.

Friedman, J.H., 1991. Multivariate adaptive regression splines. Ann. Stat. 19, 1–67.

Friedman, J.H., 2001. Greedy function approximation: a gradient boosting machine. Ann. Stat. 29, 1189–1232.

Gaser, C., Franke, K., Klöppel, S., Koutsouleris, N., Sauer, H., Alzheimer's Disease Neuroimaging, I., 2013. BrainAGE in mild cognitive impaired patients: predicting the conversion to Alzheimer's disease. PLoS One 8, e67346.

Gong, G., He, Y., Chen, Z.J., Evans, A.C., 2012. Convergence and divergence of thickness correlations with diffusion connections across the human cerebral cortex. Neuroimage 59, 1239–1248.

Good, C.D., Johnsrude, I.S., Ashburner, J., Henson, R.N.A., Fristen, K.J., Frackowiak, R.S.J., 2002. A Voxel-Based Morphometric Study of Ageing in 465 Normal Adult Human Brains, Biomedical Imaging. 5th IEEE EMBS International Summer School on, p. 16. https://ieeexplore.ieee.org/document/1233974.

Graybill, F.A., 1976. Theory and Application of the Linear Model. https://openlibrary.org/books/OL5212865M/Theory_and_application_of_the_linear_model.

Gutierrez Becker, B., Klein, T., Wachinger, C., 2018. Gaussian process uncertainty in age estimation as a measure of brain abnormality. Neuroimage 175, 246–258.

Hoerl, A.E., Kennard, R.W., 1970. Ridge regression: biased estimation for nonorthogonal problems. Technometrics 12, 55–67.

Hsu, J.-L., Leemans, A., Bai, C.-H., Lee, C.-H., Tsai, Y.-F., Chiu, H.-C., Chen, W.-H., 2008. Gender differences and age-related white matter changes of the human brain: a diffusion tensor imaging study. Neuroimage 39, 566–577.

Hui, Z., Trevor, H., 2005. Regularization and variable selection via the elastic net. J. R. Stat. Soc. Ser. B Stat. Methodol. 67, 301–320.

Jung, Y., 2012. Vessel Encoded Arterial Spin Labeling Using Fourier Encoding. 20th International Society of Magnetic Resonance in Medicine Scientific Meeting, Melbourne, Australia, p. 581.

Kirk-Sanchez, N.J., McGough, E.L., 2014. Physical exercise and cognitive performance in the elderly: current perspectives. Clin. interventions Aging 9, 51.

Koch, W., Teipel, S., Mueller, S., Buerger, K., Bokde, A.L.W., Hampel, H., Coates, U., Reiser, M., Meindl, T., 2010. Effects of aging on default mode network activity in resting state fMRI: does the method of analysis matter? Neuroimage 51, 280–287.

Kuhn, M., Johnson, K., 2013. Applied Predictive Modeling. Springer. https://www.springer.com/gp/book/9781461468486.

Kumar, R., Delshad, S., Woo, M.A., Macey, P.M., Harper, R.M., 2012. Age-related regional brain T2-relaxation changes in healthy adults. J. Magn. Reson. Imaging 35, 300–308.

Lemaitre, H., Goldman, A.L., Sambataro, F., Verchinski, B.A., Meyer-Lindenberg, A., Weinberger, D.R., Mattay, V.S., 2012. Normal age-related brain morphometric changes: nonuniformity across cortical thickness, surface area and gray matter volume? Neurobiol. Aging 33, 617.e611-617.e619.

Leo, B., Friedman, J.H., Olshen, R.A., Stone, C.J., 1984. Classification and Regression Trees. Wiley, Hoboken, NJ.

Li, H., Satterthwaite, T.D., Fan, Y., 2018. Brain Age Prediction Based on Resting-State Functional Connectivity Patterns Using Convolutional Neural Networks, 2018 IEEE 15th International Symposium on Biomedical Imaging (ISBI 2018). IEEE, pp. 101–104 arXiv:1801.04013.

Liem, F., Varoquaux, G., Kynast, J., Beyer, F., Kharabian Masouleh, S., Huntenburg, J.M., Lampe, L., Rahim, M., Abraham, A., Craddock, R.C., Riedel-Heller, S., Luck, T., Loeffler, M., Schroeter, M.L., Witte, A.V., Villringer, A., Margulies, D.S., 2017. Predicting brain-age from multimodal imaging data captures cognitive impairment. Neuroimage 148, 179–188.

MacDonald, M.E., Dolati, P., Mitha, A.P., Eesa, M., Wong, J.H., Frayne, R., 2015. Measurement of pressure and flow alterations in a giant cerebral aneurysm treated with a pipeline stent using MR imaging. Radiol. Case Rep. 10, 1109.

MacDonald, M.E., Dolati, P., Mitha, A.P., Wong, J.H., Frayne, R., 2016. Flow and pressure measurements in aneurysms and arteriovenous malformations with phase contrast MR imaging. Magn. Reson. Imaging 34, 1322–1328.

MacDonald, M.E., Forkert, N.D., Hanganu, A., Ma, Y., Williams, R.J., Sun, H., Stafford, R., McCreary, C.M., Frayne, R., Pike, G.B., 2018a. Cerebrovascular Brain Aging Examined with Arterial Spin Labelling and Applied to Age Prediction. 26th ISMRM Scientific Meeting, Paris, France, p. 0188.

MacDonald, M.E., Frayne, R., 2015. Phase contrast MR imaging measurements of blood flow in healthy human cerebral vessel segments. Physiol. Meas. 36, 1517–1527.

MacDonald, M.E., Williams, R.J., Forkert, N.D., Berman, A.J.L., McCreary, C.R., Frayne, R., Pike, G.B., 2018b. Interdatabase variability in cortical thickness measurements. Cereb. Cortex bhy197-bhy197.

Mazziotta, J., Toga, A., Evans, A., Fox, P., Lancaster, J., Zilles, K., Woods, R., Paus, T., Simpson, G., Pike, B., Holmes, C., Collins, L., Thompson, P., MacDonald, D., Iacoboni, M., Schormann, T., Amunts, K., Palomero-Gallagher, N., Geyer, S., Parsons, L., Narr, K., Kabani, N., Goualher, G.L., Boomsma, D., Cannon, T., Kawashima, R., Mazoyer, B., 2001. A probabilistic atlas and reference system for the human brain: International Consortium for Brain Mapping (ICBM). Philos. Trans. R. Soc. Lond. B. Biol. Sci. 356, 1293–1322.

Michael, T., 2010. Neural networks. Wiley Interdiscip. Rev. Comput. Stat. 2, 1–8.

Nasreddine, Z.S., Phillips, N.A., Bédirian, V., Charbonneau, S., Whitehead, V., Collin, I., Cummings, J.L., Chertkow, H., 2005. The Montreal Cognitive Assessment, MoCA: a brief screening tool for mild cognitive impairment. J. Am. Geriatr. Soc. 53, 695–699.

Ogawa, A., Sakurai, Y., Kayama, T., Yoshimoto, T., 1989. Regional cerebral blood flow with age: changes in rCBF in childhood. Neurol. Res. 11, 173–176.

Ogg, R.J., Steen, R.G., 1998. Age-related changes in Brain T1 are correlated with iron concentration. Magn. Reson. Med. 40, 749–753.

Pexman, J.H.W., Barber, P.A., Hill, M.D., Sevick, R.J., Demchuk, A.M., Hudon, M.E., Hu, W.Y., Buchan, A.M., 2001. Use of the Alberta Stroke Program Early CT Score (ASPECTS) for assessing CT scans in patients with acute stroke. Am. J. Neuroradiol. 22, 1534–1542.

Quinlan, J.R., 1987. Simplifying decision trees. Int. J. Man-Machine Stud. 27, 221–234.

Quinlan, J.R., 1992. Learning with Continuous Classes, 5th Australian Joint Conference on Artificial Intelligence. World Scientific, pp. 343–348. https://www.scirp.org/(S(i43dyn45teexjx455qlt3d2q))/reference/ReferencesPapers.aspx?ReferenceID=1865452.

Quinlan, J.R., 1993. Combining Instance-Based and Model-Based Learning, Proceedings of the Tenth International Conference on Machine Learning, pp. 236–243. http://citeseerx.ist.psu.edu/viewdoc/download?doi=10.1.1.34.6358&rep=rep1&type=pdf.

R Core Team, 2018. R: A Language and Environment for Statistical Computing. R Foundation for Statistical Computing, Vienna, Austria.

Ripley, B.D., 2007. Pattern Recognition and Neural Networks. Cambridge University Press, Cambridge, United Kingdom.

Robnik-Šikonja, M., Kononenko, I., 2003. Theoretical and empirical analysis of ReliefF and RReliefF. Machine Learn. 53, 23–69.

Rodgers, Z.B., Detre, J.A., Wehrli, F.W., 2016. MRI-based methods for quantification of the cerebral metabolic rate of oxygen. J. Cereb. Blood Flow Metab. 36, 1165–1185.

Roher, A.E., Debbins, J.P., Malek-Ahmadi, M., Chen, K., Pipe, J.G., Maze, S., Belden, C., Maarouf, C.L., Thiyyagura, P., Mo, H., Hunter, J.M., Kokjohn, T.A., Walker, D.G., Kruchowsky, J.C., Belohlavek, M., Sabbagh, M.N., Beach, T.G., 2012. Cerebral blood flow in Alzheimer's disease. Vasc. Health Risk Manag. 8, 599–611.

Román, G.C., Erkinjuntti, T., Wallin, A., Pantoni, L., Chui, H.C., 2002. Subcortical ischaemic vascular dementia. Lancet Neurol. 1, 426–436.

Ruitenberg, A., den Heijer, T., Bakker, S.L.M., van Swieten, J.C., Koudstaal, P.J., Hofman, A., Breteler, M.M.B., 2005. Cerebral hypoperfusion and clinical onset of dementia: the Rotterdam study. Ann. Neurol. 57, 789–794.

Salat, D.H., Buckner, R.L., Snyder, A.Z., Greve, D.N., Desikan, R.S.R., Busa, E., Morris, J.C., Dale, A.M., Fischl, B., 2004. Thinning of the cerebral cortex in aging. Cereb. Cortex 14, 721–730.

Ségonne, F., Dale, A.M., Busa, E., Glessner, M., Salat, D., Hahn, H.K., Fischl, B., 2004. A hybrid approach to the skull stripping problem in MRI. Neuroimage 22, 1060–1075.

Ségonne, F., Pacheco, J., Fischl, B., 2007. Geometrically accurate topology-correction of cortical surfaces using nonseparating loops. IEEE Trans. Med. Imaging 26, 518–529.

Sled, J.G., Zijdenbos, A.P., Evans, A.C., 1998. A nonparametric method for automatic correction of intensity nonuniformity in MRI data. IEEE Trans. Med. Imaging 17, 87–97.

Smola, A.J., 1996. Regression Estimation with Support Vector Learning Machines. Master's Thesis. Technische Universität München. http://alex.smola.org/papers/1996/Smola96.pdf.

Steen, R.G., Gronemeyer, S.A., Taylor, J.S., 1995. Age-related changes in proton T1 values of normal human brain. J. Magn. Reson. Imaging 5, 43–48.

Stone, M., Brooks, R.J., 1990. Continuum regression: cross-validated sequentially constructed prediction embracing ordinary least squares, partial least squares and principal components regression. J. R. Stat. Soc. Ser. B Methodol. 52, 237–269.

Sun, H., Ma, Y., MacDonald, M.E., Pike, G.B., 2018. Whole head quantitative susceptibility mapping using a least-norm direct dipole inversion method. Neuroimage 179, 166–175.

Tatu, L., Moulin, T., Bogousslavsky, J., Duvernoy, H., 1998. Arterial territories of the human brain cerebral hemispheres. Neurology 50, 1699–1708.

Tian, L., Ma, L., Wang, L., 2016. Alterations of functional connectivities from early to middle adulthood: clues from multivariate pattern analysis of resting-state fMRI data. Neuroimage 129, 389–400.

Tustison, N.J., Cook, P.A., Klein, A., Song, G., Das, S.R., Duda, J.T., Kandel, B.M., van Strien, N., Stone, J.R., Gee, J.C., Avants, B.B., 2014. Large-scale evaluation of ANTs and FreeSurfer cortical thickness measurements. Neuroimage 99, 166–179.

Valizadeh, S.A., Hänggi, J., Mérillat, S., Jäncke, L., 2017. Age prediction on the basis of brain anatomical measures. Hum. Brain Mapp. 38, 997–1008.

Wang, Y., Witten, I.H., 1996. Induction of model trees for predicting continuous classes. Comput. Sci. Working Pap.

Wendell, C.R., Gunstad, J., Waldstein, S.R., Wright, J.G., Ferrucci, L., Zonderman, A.B., 2014. Cardiorespiratory fitness and accelerated cognitive decline with aging. J. Gerontol. Ser. A 69, 455–462.

Wold, H., 1966. Estimation of principal components and related models by iterative least squares. Multivariate Anal. 391–420.

Wold, S., Geladi, P., Esbensen, K., Öhman, J., 1987. Multi-way principal components- and PLS-analysis. J. Chemometrics 1, 41–56.

Wong, E.C., 2007. Vessel-encoded arterial spin-labeling using pseudocontinuous tagging. Magn. Reson. Med. 58, 1086–1091.

Zhang, Y., Brady, M., Smith, S., 2001. Segmentation of brain MR images through a hidden Markov random field model and the expectation-maximization algorithm. IEEE Trans. Med. Imaging 20, 45–57.

Zhao, M.Y., Mezue, M., Segerdahl, A.R., Okell, T.W., Tracey, I., Xiao, Y., Chappell, M.A., 2017. A systematic study of the sensitivity of partial volume correction methods for the quantification of perfusion from pseudo-continuous arterial spin labeling MRI. Neuroimage 162, 384–397.